AIAA 82-4204

Unsteady Airfoil Pressures Produced by Periodic Aerodynamic Interference

Peter F. Lorber* and Eugene E. Covert†
Massachusetts Institute of Technology, Cambridge, Mass.

An experimental study was made of the unsteady pressures induced on a two-dimensional airfoil by the rotation of an elliptical cylinder located behind and beneath the airfoil trailing edge. The experiment was conducted in a low Mach number flow for reduced frequencies based on airfoil semichord up to 6.4. Mean pressures and phases and amplitudes of the fundamental harmonic were measured and compared to predictions made using thin airfoil theory and the measured unsteady upwash produced by the rotating cylinder alone. Mean difference pressures were found to be in good agreement with the predictions. The pressure difference approached zero as the trailing edge was approached. Qualitative agreement between data and thin airfoil theory was found for the oscillating component except near the trailing edge where a difference in the phase was found.

Nomenclature

c = airfoil chord
C_p = pressure coefficient, $(p-p_\infty)/\frac{1}{2}\rho U_\infty^2$
ΔC_p = $C_{p\text{lower}} - C_{p\text{upper}}$
f = frequency, Hz
K = reduced frequency, $\omega c/2U_\infty$
Re = Reynolds number based on airfoil chord, $U_\infty c/\nu$
p = pressure
t = time
$\bar{U}$ = horizontal mean velocity along airfoil chord
U_∞ = freestream velocity
u = horizontal perturbation velocity
v = vertical perturbation velocity
x = horizontal coordinate, measured from airfoil leading edge
y = vertical coordinate, measured from airfoil chord line
α_{mean} = mean local flow angle
α_{fluct} = amplitude of oscillating flow angle
α_{else} = remainder of local flow angle
θ = orientation of elliptic cylinder, 0 deg for major axis horizontal and 90 deg for major axis vertical
ρ = density
$\Delta\Phi$ = phase lag, deg
ν = kinematic viscosity
ω = radian frequency

Introduction

UNSTEADY airfoil pressures have been generated by diverse techniques in previous studies. They have also covered a wide range of operating velocities and reduced frequencies, defined here as radian frequency times airfoil semichord divided by freestream velocity.

Commerford and Carta[1] placed a cylinder below and ahead of an airfoil. The natural shed vorticity of the cylinder induced unsteady pressures on the airfoil at a reduced frequency of $K=3.9$. Pressures were recorded at five chordwise locations and integrated to give the unsteady lift. Pressure and lift were compared to several thin airfoil theories.

Saxena et al.[2] rotated shutters downstream of a stationary airfoil to produce longitudinal flow perturbations of reduced frequencies of 0.18 and 0.9. They measured instantaneous pressure distributions. Satyanarayana and Davis[3] oscillated an airfoil about the one-quarter chord position. Unsteady pressures were obtained for reduced frequencies ranging between 0.5 and 1.2 at five chordwise locations, primarily in the trailing-edge region.

Davis and Malcolm[4] forced vertical displacement (plunging) and rotational motion of an airfoil. Unsteady and static pressures were measured at 20 chordwise locations for reduced frequencies ranging over $K=0.026$-0.25. Averaged pressure distributions were reported for the various high subsonic and transonic flow regimes.

Finally, Fleeter[5] studied unsteady pressures near the trailing edge of fixed stators perturbed by the rotor wakes in a large low-speed compressor. The behavior for cambered and uncambered blades at various incidence angles was studied at fundamental reduced frequencies near 8.0.

The previous discussion and the summary in Table 1 suggest that the diverse range of situations studied has resulted in a similarly diverse set of conclusions. Overall, however, two trends were noticed. First, in all but one of the cases discussed, the unsteady difference pressure approached zero at the airfoil trailing edge. This is also true of Fleeter's flat-plate cascade data.[5] The exception was the result for a cambered airfoil cascade also reported in Ref. 5. Here, difference pressure amplitudes increased from $x/c=0.90$ to 0.97. However, the transducers on the suction surface were located on one airfoil in the cascade and the pressure surface transducers on a second, so the data may contain phase differences that are not well defined.

The second trend was lack of quantitative agreement between thin airfoil theory predictions and experimental results for difference pressure amplitudes and phases as reduced frequencies increased beyond $K=0.5$ (1,3,4,5). The reduced frequency in these data is of limited range and lacks continuity between the diverse experiments.

The present study provides data over a comparatively wide range of chordwise pressure-measuring locations and reduced frequencies. In this study the airfoil is stationary and a nonuniform nonsteady upwash drives the flow. Hence, no acceleration correction is required for the transducers. Steady-state measurement of parameters using the present concept was reported in Refs. 6 and 7.

Experimental Apparatus

The experiment described above was performed in MIT's Wright Brothers Memorial Wind Tunnel. This tunnel has an

Received Feb. 23, 1981; revision received Jan. 4, 1982.

*Graduate Research Assistant. Student Member AIAA.
†Professor of Aeronautics and Astronautics, Director of Gas Turbine and Plasma Dynamics Laboratory. Fellow AIAA.

Table 1 Summary of unsteady airfoil data

Reference	1	2	3	4	5	Present
Airfoil	Circular arc	NACA 0012	NACA 64A010	NACA 64A010	NACA 65 series	NACA 0012
Type of perturbation	Vorticity shed from cylinder	Downstream shutters	Pitching airfoil	Pitching and plunging airfoil	Compressor rotors	Rotating elliptical cylinder
Convected disturbance?	Yes	No	No	No	Mostly	No
Mach number	0.25	0.03	0.17	0.5-0.8	0.03	0.03-0.09
Reduced frequency $k^2M^2/(1-M^2)$	3.9 0.67	0.18-0.9 <0.0007	0.05-1.2 <0.04	0.026-0.255 0.32	7.5-10.1 0.09	0.5-6.4 0.30
Pressure tap locations, X/c	0.10-0.90	0.0-0.82	0.4, 0.89-0.973	0.3-0.94	0.90-0.97	0.0-0.98
ΔC_p $(X/c=1)$-->?	0	0	0	0	0 for flat plate in cascade and isolated, $\neq 0$ for cambered cascade	0
Unsteady difference pressure and theory:						
Amplitude	Experiment greater	—	Experiment less, more difference for $K>0.8$	"Good" agreement for subsonic	Experiment greater than theory, esp. for cambered cascade	Experiment less than theory; differences increased with K
Phase	Experimental chordwise variation greater than theory	—	Experiment less than theory more difference for $K>0.8$	"Good" agreement for subsonic	Fair	Fair away from trailing edge

elliptical test section with axes 2.3×3.0 m (7.5×10 ft). Turbulence levels encountered in the freestream of this tunnel are relatively high, typically about 0.5-1.0%. Noise at the fan blade passing frequency and its harmonics may also be significant for velocities 10 m/s or below.

A NACA 0012 airfoil section of 51 cm (20 in.) chord was mounted at zero angle of attack between two sidewalls extending from top to bottom and in the center of the test section. The leading edge of the sidewalls was one-half chord ahead of the leading edge of the airfoil. The solid sidewalls diverged slightly in the downstream direction to compensate for the average growth of the boundary-layer displacement thicknesses.‡ Also, all joints between airfoil and sidewalls were sealed to prevent leaks and secondary flows.

The unsteady perturbation was provided by rotating an elliptic cylinder located behind and beneath the airfoil trailing edge. The semimajor axis of the ellipse was 6.9 cm (2.7 in.) or 0.136 chord. The semiminor axis was 0.061 chord. The axis of rotation of the body was located at $x/c=1.175$, $y/c=-0.276$. At closest approach the ellipse-trailing edge separation was 0.15 chord with the semimajor axis rotated 58 deg clockwise from the horizontal. Roughness was applied to the cylinder in order to delay separation on its surface and to increase its repeatability. A variable-speed dc motor rotated the cylinder at 90-3000 rpm.

A schematic diagram of the wind-tunnel test section during an airfoil surface pressure test is shown in Fig. 1.

The unsteady increment of velocity produced by the rotating elliptical cylinder without the airfoil in the tunnel was measured in the plane of the chord. Horizontal and vertical flow velocities were measured with a constant-temperature cross hot wire using Flow Corporation 900 series components. The quotient of the difference of the two wires over their sum was calibrated in terms of the local flow angle. The reference conditions were defined as those existing when an elliptical cylinder has its major axis aligned with the wind (horizontal). An implicit assumption is made here: the unsteady upwash distribution is unaltered by adding the airfoil, i.e., the influence of the airfoil on the flow over the ellipse results in a negligible effect on the upwash distribution. This seems valid in most cases. See the Appendix for further discussion.

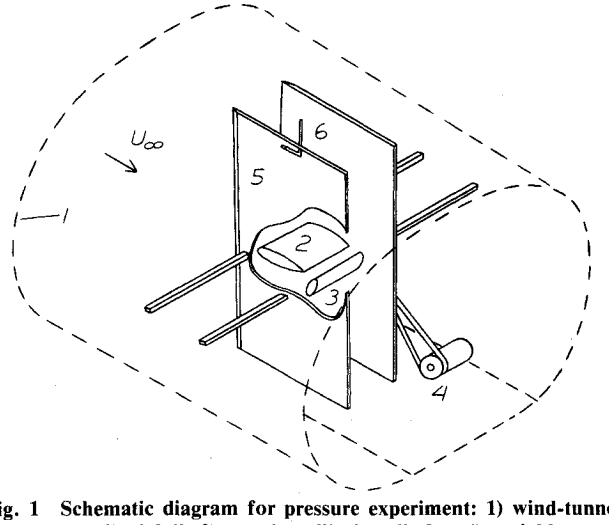

Fig. 1 Schematic diagram for pressure experiment: 1) wind-tunnel test section, 2) airfoil, 3) rotating elliptic cylinder, 4) variable speed motor, 5) sidewalls, 6) pitot-static tube.

The second set of measurements involved airfoil surface pressures. The upper and lower surfaces were each fitted with 17 pressure taps, with a 35th tap being located at the leading edge. The taps of each surface were connected via 25-28 cm long tubing to a Scanivalve rotary valve. Each tube was fitted with individually sized and positioned yarn inserts to avoid resonances in the frequency band of interest. Setra model 237 capacitive pressure transducers were used to get the mean and unsteady pressures for each Scanivalve.

This pressure system was calibrated for both amplitude and phase. The procedure was to compare the response of the operational tubing, yarn, and Scanivalve system with that of a bare diaphragm transducer, which was known to have a flat response up to well above the 1000 Hz maximum frequency of present interest. The amplitude response was flat to 600 Hz, dropping to 60% at 950 Hz.

‡The wall divergence angle was determined experimentally by measurements of pressure distribution on a flat plate.[6] The leading edge was beveled on the outside of the sidewalls.

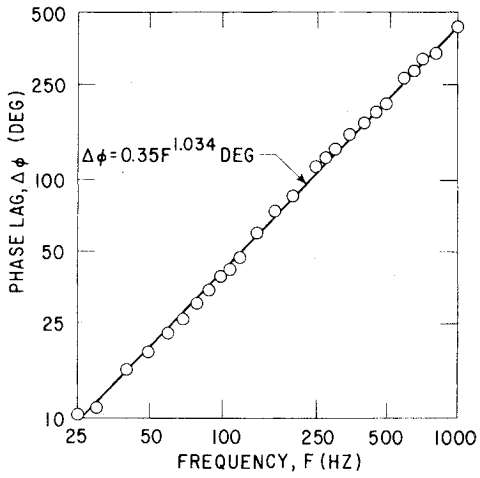

Fig. 2 Phase lag calibration for pressure system.

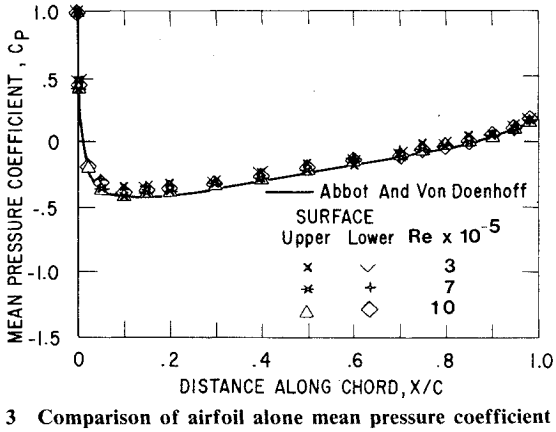

Fig. 3 Comparison of airfoil alone mean pressure coefficient with previous results for NACA 0012.

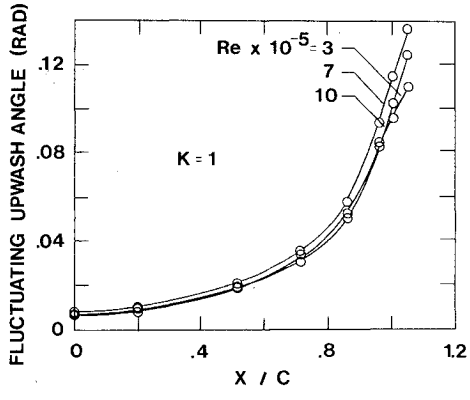

Fig. 4 Amplitude of oscillating induced upwash for reduced frequency, $K = 1$.

Figure 2 illustrates the lag in phase of the operational system as compared to the reference transducer. Over the range shown a least squares fit to the data resulted in

$$\Delta\Phi = 0.35[f(\mathrm{Hz})]^{1.03} \text{ deg}$$

This corresponds to a time delay in the lines varying with frequency of 1.05-1.25 ms.

Pressures were nondimensionalized using the mean dynamic pressure obtained from a pitot-static probe located approximately one chord length above the airfoil between the sidewalls. This pitot-static tube determined the tunnel conditions. Figure 3 shows a comparison of the measured

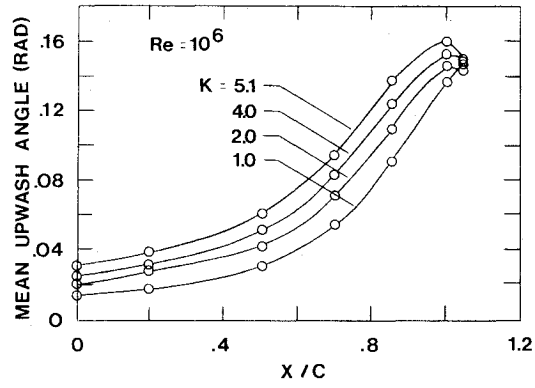

Fig. 5 Mean of induced upwash for reduced frequencies, $K = 1, 2, 4, 5.1$.

pressure (coefficient) distribution on the airfoil, in the absence of the elliptic cylinder, with the distribution of pressure coefficient in Ref. 8. The agreement is good. Thus, this location of the pitot provided an accurate reference velocity, including blockage effects.

The analog data analysis procedure was quite similar for both velocity and pressure signals. The principal unsteady measurements were the phase-locked averaged waveforms obtained using an eductor. This device was synchronized by a pulse train produced by a photoelectric sensor viewing the elliptical cylinder shaft. The eductor divided each revolution into 100 intervals and averaged each interval over a time typically corresponding to 100 revolutions. This averaging process reduced the noise and the amplitude of signals whose frequency content was not an integral multiple of the excitation. The graphical output produced was later analyzed for amplitude and phase of the fundamental harmonic.

In addition to the phase lock averaging, time averages, root mean square values, and power spectral densities were also determined.

Results of Induced-Velocity Tests

For present purposes the ideal waveform of the upwash would be a pure sinusoid of frequency equal to twice the cylinder rotation frequency. Also the amplitude of the fluctuating upwash should be as large as possible near the trailing edge. The best approximation to these criteria resulted from rotation of a rough-surfaced cylinder in the clockwise direction. In other words, the circulation-induced velocity is an upwash in front of the cylinder. A more detailed discussion of the flow about the rotating cylinder, the effect of the interference on separation on the elliptic cylinder, and the resulting form of the upwash is given in Ref. 9. An abridged discussion of one of these effects, as seen in both upwash and pressure measurements, is contained in the Appendix.

The results of the velocity tests that are of primary importance for the present purposes are plots of the mean upwash and the amplitude of the fundamental frequency vs distance, along the position of the airfoil chord. Figures 4 and 5 show this information for typical cases. The first shows the fluctuating amplitude at frequency $K = 1$ for the three Reynolds numbers. The second shows the mean induced angle at a Reynolds number of a million for four reduced frequencies. Mean flow angles were found by dividing the mean vertical velocity by the mean horizontal velocity, applying calibration corrections, and interpreting as angles in radians. Fluctuating flow angle amplitudes were determined from the division of the phase lock-averaged vertical velocity by the mean horizontal velocity at that chordwise position. The local flow angle then became

$$\alpha(x, y=0, t) = \alpha_{\text{mean}}(x) + \alpha_{\text{fluct}}(x)\sin[\omega t - \Phi(x)] + \alpha_{\text{else}}(x, t)$$

where α_{else} is the angle of attack due to noise, turbulence, and higher harmonics and is typically half a degree or less. Ensemble averaging was used to reduce turbulence and noise to a negligible level. The effects of higher harmonics were removed by spectral analysis of the data. $\Phi(x)$ is the phase lag with respect to the elliptical cylinder.

Note the chordwise distribution is essentially independent of Reynolds number (Fig. 4). In particular, the difference among fluctuating amplitudes was of the same order or less than the estimated probable error for those measurements of 0.1 deg (0.002 rad). With regard to the mean, the difference between velocities was somewhat greater, as was the probable error of 0.4 deg (0.007 rad). However, the actual angle was used in each case for the calculations.

The final characteristic of the induced velocity field to be discussed is the phase lag. Phase lag is defined as the difference between the time when the major axis of the elliptical cylinder is horizontal and the time of the minimum of the studied quantity. This time interval is then converted to degrees through the use of the angular velocity of the cylinder, producing 720 deg per revolution. The maximum phase lag in the induced velocity was at the trailing-edge position, where a lag of 25-30 deg was seen for higher frequencies. The phase decreased by between 15 and 20 deg as the hot wire was moved forward to 70% of chord position. As the hot wire was moved to a more forward position on the airfoil the change in the phase was small and was often hard to interpret because of the low signal amplitudes near the leading-edge position. Errors in phase lag were at most 3-5 deg.

Application of Induced-Velocity Data

The measured upwash distributions were used with linearized thin airfoil theory to predict unsteady difference pressures. Since the disturbances were fixed to the airfoil frame of reference (the maximum upwash was always at the trailing edge, regardless of the phase), Theodorsen's theory[10,11] was used instead of the Sears theory.[12,13] §

The key assumptions in the Theodorsen theory are potential flow, wake vorticity that is convected downstream at the mean velocity, a linearization of the upwash boundary conditions and of the Bernoulli equation, and most importantly that the product $[u]\cdot\sqrt{x}\cdot(c-x)$ approaches zero at the trailing edge. This last condition is sufficient to ensure finite velocities at the trailing edge. In addition to these assumptions in the basic theory, it was necessary to add a further approximation: that the phase of the upwash was constant over the airfoil chord. This constant was chosen to represent the phase in the maximum amplitude region near the trailing edge. Finally, a Van Dyke type of correction was applied to account for the rounded leading edge.[14] (The effect of the test section walls on the Theodorsen function was estimated to be approximately 1% or less.[15])

Results of Pressure Tests

The first class of pressure results involved surface pressure coefficients. Figures 6 and 7 show these data for three Reynolds numbers with the elliptical cylinder major axis fixed in the horizontal and vertical directions, respectively. The data show that the pressure distribution is essentially independent of the Reynolds number. Note the difference in increasing pressure gradients on the rear upper surfaces as a function of the cylinder angular position. Detailed pressure distribution data are available in Ref. 9.

§The Sears theory considers convected disturbances of the form exp $[i\omega(t-x/U_\infty)]$. A preliminary analysis was made assuming the upwash was the sum of a fixed-phase component (Theodorsen) and a traveling wave component (Sears). The latter was represented by a sum of a number of harmonics that varied from case to case, but seemed to represent a converged representation in every case. The contributions of the traveling wave upwash to the unsteady pressure distribution was of the order of the uncertainty in the measurement of unsteady pressure for the conditions reported here.

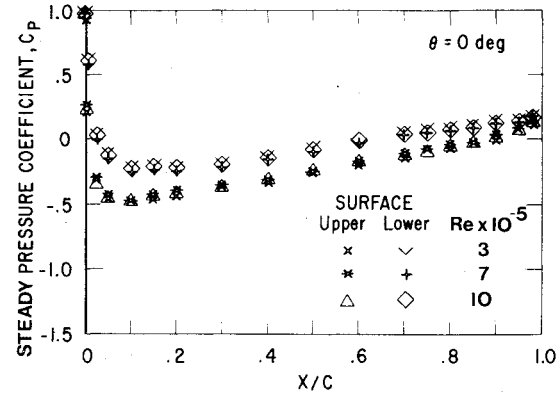

Fig. 6 Steady airfoil surface pressure coefficients for elliptical cylinder major axis in horizontal position.

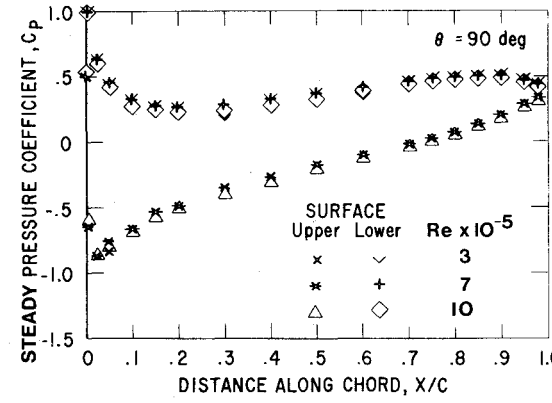

Fig. 7 Steady airfoil surface pressure coefficients for elliptical cylinder major axis in vertical position.

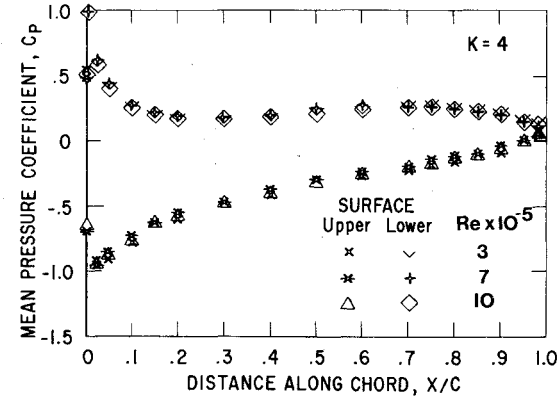

Fig. 8 Mean airfoil surface pressure coefficients for elliptical cylinder rotating at $K=4$.

The mean pressure for rotational reduced frequency $K=4$ is shown in Fig. 8. Note the data are essentially independent of Reynolds number for this range. In general the mean pressures behaved similarly to the quasisteady pressures, representing an average over the various steady elliptical cylinder orientations. The difference between the static pressure coefficient shown in Figs. 6 and 7 and the mean averaged pressure coefficient shown in Fig. 8 was a mean difference pressure resulting from the rotational circulation, which increased with reduced frequency.

A comparison of the mean difference pressure for $K=4.0$ and Reynolds number 1×10^6 with the upwash-based prediction is given in Fig. 9. As was the case with most of the other 11 speed-frequency combinations studied, the agreement seemed quite good over the middle 90% of the

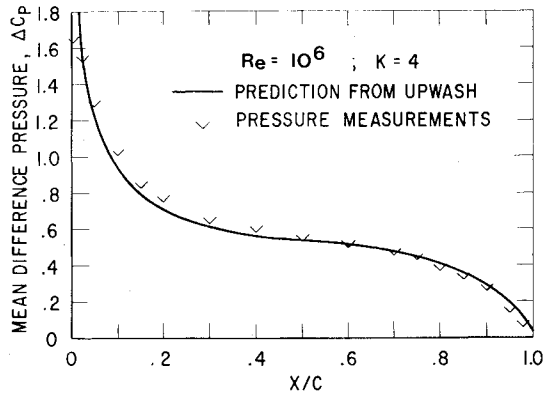

Fig. 9 Typical comparison of mean difference pressure coefficient measurements with upwash-based prediction.

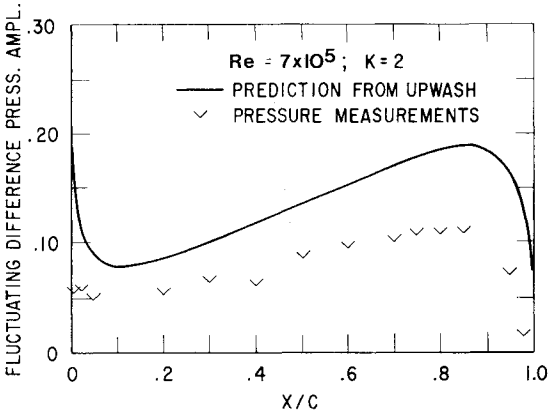

Fig. 10 Typical comparison of fluctuating difference pressure amplitude phase lock averaged measurements with upwash-based prediction.

chord. The trailing-edge difference pressures were seen to approach zero somewhat more gradually than the prediction.

The calculated and measured fundamental harmonics of the fluctuating pressure coefficient amplitude are shown in Fig. 10. The qualitative features were similar, regarding the locations of minima and maxima and the general shape of the curve, but the magnitude was sizeably overpredicted. This overprediction increased with reduced frequency, ranging from 20-30% for $K=1$ to 60% for $K=6.4$.¶ The maximum at the leading edge decreased in amplitude with increased reduced frequency. The maximum also moved forward under these circumstances. Amplitudes of the maximum near $x/c=0.85$ started at $C_p=0.16$ for $K=1.0$, dropped to $C_p=0.08$-0.10 at $K=2.0$, and then increased to $C_p=0.13$ by $K=6.4$.

Figure 11 shows the phase lag for the difference pressure coefficient fundamental at 20 m/s and $K=2.0$. The measurements were made with the same procedure used for the induced-velocity phases, resulting in a probable error in the data for each speed frequency combination of 2-5 deg. A phase bias may have existed between pressure data at different speed frequency combinations and between the pressure data and the predictions. This bias comes about because the phase of the unsteady upwash distribution is not constant near the trailing edge, as mentioned previously.

¶The difference between the prediction and the measurement is probably due to basic limitations resulting from the assumptions underlying the unsteady thin airfoil theory, because the contribution from traveling wave part of the upwash is an order of magnitude smaller than this difference. The authors would like to thank the reviewers for a stimulating series of questions on this point.

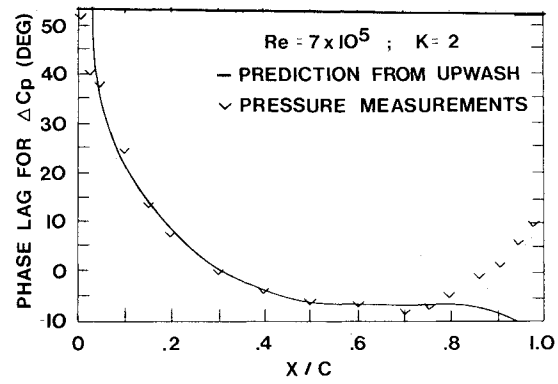

Fig. 11 Typical comparison of difference pressure phase lag with respect to elliptical cylinder measurements with upwash-based prediction.

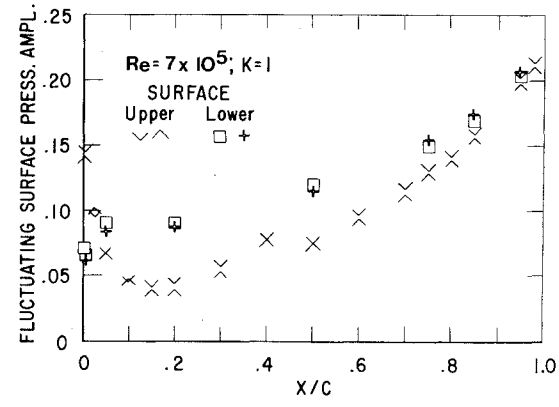

Fig. 12 Typical lower frequency fluctuating surface pressure amplitude (the two sets of points given for each surface are data for the two half periods) (see Appendix).

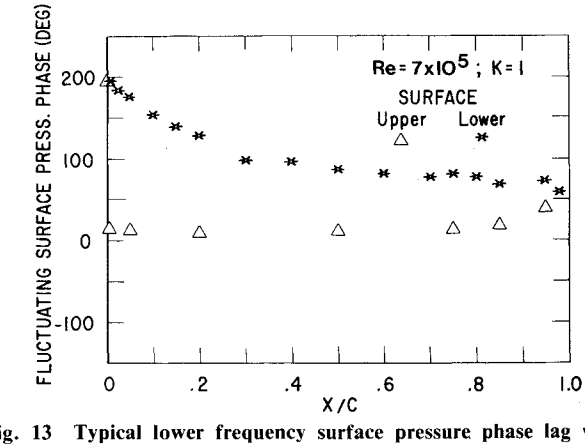

Fig. 13 Typical lower frequency surface pressure phase lag with respect to elliptical cylinder.

Over the trailing-edge region the measured phase differed markedly from the prediction. The predicted phase approached a lead of 90 deg in advance of the upwash velocity in contrast to the near zero phase lag actually observed over the final portion of the airfoil chord.**

The differences between the assumptions underlying Theodorsen's work and the experimental conditions are striking. The trailing-edge geometry of the NACA 0012 used

**One of the reviewers suggested this may be due to separation near the trailing edge. Examination of the velocity profile at 94% of the chord over the period shows no inflection point. The flow is likely to be attached. Nevertheless, this trailing-edge effect is likely to be a viscous coupled phenomenon.

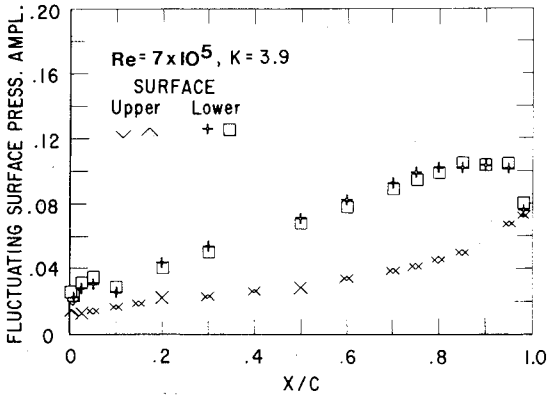

Fig. 14 Typical higher frequency fluctuating surface pressure amplitude.

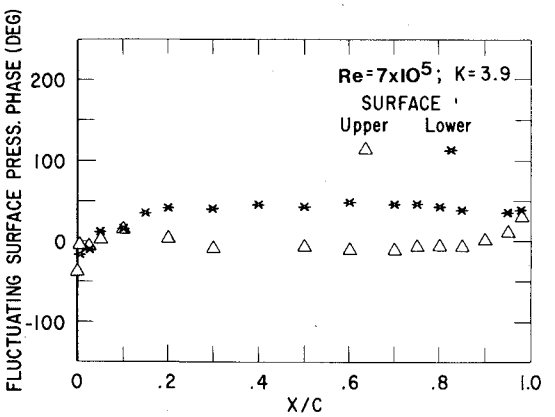

Fig. 15 Typical higher frequency surface pressure phase lag with respect to elliptical cylinder.

here had a finite-thickness trailing edge and an included angle equal to 16 deg, not a cusp. Increasing the trailing-edge angle decreases the lift curve slope[8] so that the lower than predicted response in terms of difference pressures to the induced-upwash perturbation might have been due partly to the finite trailing-edge angle.

The assumption of potential flow near the trailing edge, a region marked by thick boundary layers and a viscous wake, was also unrealistic. The effect may be magnified by the fact that the main perturbation created by the rotating elliptical cylinder occurred in just this trailing-edge region.

The final class of results to be considered are the actual fluctuating surface pressures. Figures 12 and 13 show the amplitude and phase for the case of Reynolds number of 7×10^5 and reduced frequency $K=1$.

Figures 14 and 15 show the equivalent data for $K=3.9$. Note the significant differences between the unsteady pressure data at this higher value of K and the data at $K=1$ (Figs. 12 and 13). First, the amplitudes were generally lower, and the upper and lower surfaces join in a more rounded shape. The phase behavior exhibited a more drastic shift. The leading-edge phase peak has vanished to be replaced by negative phases on the upper and lower surface. Over the rear of the airfoil, however, the phase maintained a form similar to the low-frequency cases. Although no explanation for this shift yet exists, several points may be made. First, both amplitude and phase behavior shifts occurred near the dimensionally reasonable reduced frequency $K=1$. Second, Franke and Henderson[16] also observed a large phase shift near the leading edge of the suction surface of an airfoil at high ($K=5$) reduced frequency.

Conclusions

1) Mean airfoil surface pressure distributions were found to have smooth gradients and to depend primarily on the reduced frequency.

2) Mean difference pressures were in good agreement with predictions based on the measured upwash induced by the elliptic cylinder.

3) The fundamental harmonic of the surface pressures were well behaved over the rear portion of the airfoil. The distribution of unsteady pressure was different as the reduced frequency was above or below $K=1.5$.

4) Fluctuating difference pressure amplitudes and phases were in qualitative agreement with the predictions, except for the trailing-edge phase behavior. Amplitudes were increasingly overpredicted as reduced frequency increased.

5) Difference pressure amplitudes approached zero at the trailing-edge position.

6) Difference pressures depended primarily upon the reduced frequency at a fixed angle of attack.

Appendix: Unsteady Coupling between the Rotating Ellipse and the Airfoil

For most of the range of reduced frequencies and Reynolds number the measured pressure distribution bore a close relation to that predicted on the basis of the measured upwash distributions. This seemed to imply the airfoil had only a weak coupling with the flow over the ellipse.†† During the upwash measurements that were made with only the rotating elliptic cylinder in the tunnel, some anomalies in the upwash chordwise distribution were observed at certain reduced frequencies. These reduced frequencies were in the test matrix.

The atypical situation is shown in Fig. A1. It shows the phase lock-averaged induced upwash velocity over one elliptical cylinder period. The upper figure is for reduced frequency $K=5.99$, and shows a large difference in the behavior during the two half periods. The lower figure is for $K=6.28$, with all other conditions identical. The difference has been substantially reduced.

As a matter of practice, these frequencies were avoided when taking data. Thus, we used 3.9 instead of 4, and 6.3 and 6.4 instead of 6.0. A quick survey indicated that frequencies near these where the waveform lacked symmetry resulted in pressure distributions with large differences between one half revolution and the other half revolution. The latter result also suggests a weak influence of the flow over the airfoil on the unsteady characteristics of the separation on the ellipse.

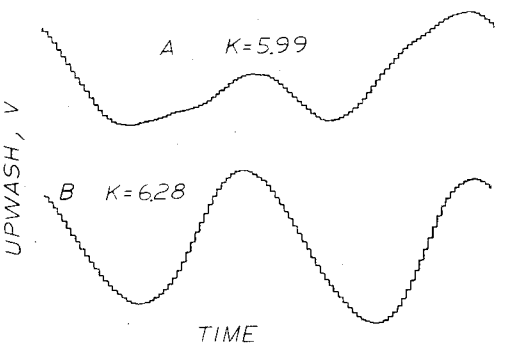

Fig. A1 Frequency effect on upwash velocity waveform, $x/c=1.0$, $Re=7\times10^5$.

††In response to questions raised by a reviewer of this paper, a series of smoke flow (streak line) photographs was made of the wake behind the rotating ellipse with and without the airfoil. These photographs show that the airfoil had a negligible effect on the streak line shape, to within the repeatability of the streak line position.

Acknowledgments

This work was performed for the Mechanics Branch of the U.S. Air Force Office of Scientific Research under Contract F49620-79-C-0226, Capt. Michael Francis, Project Monitor.

References

[1] Commerford, G. L. and Carta, F. O., "Unsteady Aerodynamic Response of a Two-Dimensional Airfoil at High Reduced Frequency," *AIAA Journal*, Vol. 12, Jan. 1974, pp. 43-48.

[2] Saxena, L. S., Fejer, A. A., and Morkovin, M. V., "Features of Unsteady Flows over Airfoils," AGARD CP-227, 1978, pp. 22-1-22-11.

[3] Satyanarayana, B. and Davis, S., "Experimental Studies of Unsteady Trailing Edge Conditions," *AIAA Journal*, Vol. 16, Feb. 1978, pp. 125-129.

[4] Davis, S. S. and Malcolm, G. M., "Experiments in Unsteady Transonic Flow," AIAA Paper 79-0769, April 1979.

[5] Fleeter, A., "Trailing Edge Conditions for Unsteady Flows at High Reduced Frequency," *AIAA Journal*, Vol. 18, May 1980, pp. 497-503.

[6] Kanevsky, A. R., "Comparison of the Pressure Distribution for Circulation Generated by Angle of Attack with that Generated by Trailing Edge Perturbation," S.M. Thesis, Dept. of Aeronautics and Astronautics, MIT, Cambridge, Mass., Feb. 1978.

[7] Cervisi, R. T., "Turbulent Boundary Layer on an Airfoil in Several Adverse Pressure Gradients," S.M. Thesis, Dept. of Aeronautics and Astronautics, MIT, Cambridge, Mass., Sept. 1978.

[8] Abbott, I. H. and von Doenhoff, A. E., *Theory of Wing Sections*, Dover Publications, New York, 1959, pp. 130-131, 321.

[9] Lorber, P. F., "Unsteady Airfoil Pressures Induced by Perturbation of the Trailing Edge Flow," S.M. Thesis, Dept. of Aeronautics and Astronautics, MIT, Cambridge, Mass., Feb. 1981.

[10] Theodorsen, T., "General Theory of Aerodynamic Instability and the Mechanics of Flutter," NACA Rept. 496, 1934.

[11] Bisplinghoff, R. L., Ashley, H., and Halfman, R. L., *Aeroelasticity*, Addison-Wesley Publishing Co., Reading, Mass., 1955, pp. 251-281.

[12] Sears, W. R., "Some Aspects of Non-Stationary Airfoil Theory and Its Practical Application," *Journal of the Aeronautical Sciences*, Vol. 8, 1941, pp. 104-108.

[13] Commerford, G. L. and Carta, F. O., "An Exploratory Investigation of the Unsteady Aerodynamic Response of a Two-Dimensional Airfoil at High Reduced Frequency," AIAA Paper 73-309, 1973.

[14] Van Dyke, M., *Perturbation Methods in Fluid Mechanics*, Academic Press, New York, 1964, pp. 59-61.

[15] Rock, S. M. and DeBra, D. B., "Prediction and Experimental Verification of Transient Airfoil Motion," *Journal of Aircraft*, Vol. 19, June 1982, pp. 456-464.

[16] Franke, G. F. and Henderson, R. E., "Unsteady Stator Response to Upstream Rotor Wakes," *Journal of Aircraft*, Vol. 17, July 1980, pp. 500-507.